

Fe(III) Detection by Multicolor Carbon Dots as Fluorometric Probes

N. Alvandi¹, Z. Ranjbar², N. Esfandiari*¹

¹ Department of Life Sciences and Biotechnology, Shahid Beheshti University, P.O. Box: 1983969411, Tehran, Iran.

² Department of Surface Coatings and Corrosion, Institute for Color Science and Technology, P.O. Box: 1668836471, Tehran, Iran.

ARTICLE INFO

Article history:

Received: 15 May 2023

Final Revised: 12 July 2023

Accepted: 15 July 2023

Available online: 14 Oct 2023

Keywords:

Fe(III) detection

Multicolor carbon dots

Ultra-low detection limit

Nanobiosensors

ABSTRACT

*T*aking an industrial standpoint, the recognition of Fe(III) as a heavy metal ion can exert a profound impact on the industry. In this research, we synthesized carbon dots from a novel and local green source by hydrothermal method. Afterwards, characterization tests, like dynamic light scattering, zeta potential sizer, atomic force microscopy, Fourier transform infrared spectroscopy, X-ray powder diffraction, elemental analysis, and transmission electron microscopy have been done. After investigation of physicochemical properties, the proposed novel nanobiosensor based on multicolor carbon dots can detect Fe(III) with ultra-low detection limit compared with other studies. The designed nanobiosensor does not identify other ions, confirming its detection specificity. Besides, this nanobiosensor can detect Fe(III) ion in two different conditions, tap water and cysteine solution as real samples. This accurate and sensitive detection of Fe(III) in different conditions can play an impressive role in industries in the near future. *Prog. Color Colorants Coat. 17 (2024), 11-25* © Institute for Color Science and Technology.

1. Introduction

During recent years, we were witness of industrial development as a forerunner in every aspect of human life [1, 2]. Consequently, industrial pollution and their effects on the environment and human food chains have been considered as a global concern. Heavy metal pollution as a kind of industrial pollutions has become a serious economic and social problem [3]. These heavy metal ions are discharged into the drinking water and the human food chains. Afterward, they gradually enriched in human tissues and organs. Herein, mankind's health can be significantly affected by the low levels of heavy metal ions and the detection of them should be considered as a crucial factor. In addition, industrial applications can benefit from heavy metal ions determination [4-6]. This kind of detection can lead to the industrial products change, for instance corrosion process which causes the gradual destruction

in different industrial goods can be controlled by Fe detection [7].

For this purpose, innumerable monitoring approaches for Fe ions detection have been developed, such as potentiometric sensors, ion selective electrodes (ISEs), atomic absorption spectrometry (AAS), inductively coupled plasma mass spectrometry (ICP-MS), inductively coupled plasma-atomic emission spectrometry (ICP-AES), chromatographic separation, and etc. These proposed methods have some demerits. For instance, these methods are expensive and need expert operators [8]. In addition, a careful sample preparation should be needed. Hence, the lack of a novel, cost-effective, and more sensitive detection method for Fe ions determination has been realized [9].

In this situation, nanotechnology which can be used in multitudes scopes [10-16] is capable of playing a crucial role in heavy metal ions detection [17-19].

*Corresponding author: * ne_esfandiari@sbu.ac.ir

Doi: 10.30509/pccc.2023.167138.1218

Carbon dots (CDs) as a categorization of nanomaterials ranging less than 10 nm can be considered as suitable candidate in this field [20]. They have received much attention due to their physicochemical properties [21], like optical and electrochemical features, high surface-to-volume ratio, favorable biocompatibility, low cytotoxicity, ultra-low detection limit, simple surface functionalization, high electron mobility, and etc. [22]. Carbonization as an efficient and necessary process [23] is occurred by common synthesis methods, such as hydrothermal treatments, electrochemical oxidation, ultra-sonication, laser ablation, microwave approaches, and many more [24]. CDs can be also synthesized by different sources from chemical to green by hydrothermal method [25]. This feature can be considered as one of the significant properties of CDs [26].

Optical-based sensors with “ON-OFF” sensing platform have been preferred because they can be quenched rapidly in response to binding with targeted analytes by an acclaimed fluorescence-quenching strategy [27]. During recent years, CDs can be considered as effective fluorescent nanoprobe and much focus has been attracted to their use as “ON-OFF” sensors [20, 28] so as to detect various analytes due to their fantastic features, such as miniscule size, unique morphology, the capability of multi-fluorescence color emission [29], and fondness of fluorescence-quenching mechanism [30]. Furthermore, their detection can be recognized by the clear optical signal that this can be regarded as another significant feature of CDs. Besides, multicolor CDs have been synthesized by different approaches, such as changing the size, functional groups, and synthesis sources of CDs. Another novel method for multi-color CDs synthesis is changing of their concentrations reported by other papers [20, 28].

In this research, a new-designed “ON-OFF” biosensor based on multicolor concentration-dependent CDs with pH-sensitive behavior is reported. The eco-friendly and novel carbon source of synthesized CDs in this study is a specific variant of greengage (*Prunus italica Borkh*) from the Rosaceae family which grows in specific part of Iran and never has been still used as a CDs source. CDs derived from this green source can detect Fe(III) ions by a fluorescence-quenching strategy with ultra-low detection limit. Fe(III) can be considered as a kind of environmental pollutant and its detection can remove it from food chains of humans

and animals which make Fe(III) determination so efficient and crucial [31]. Furthermore, the specificity of our designed nanobiosensor was justified and its advantages were validated in the tap water and cysteine solution samples.

2. Experimental

2.1. Reagents and instruments

Proposed green source in this study has been supplied from the local garden located in Hamedan, Iran. Moreover, metal ions, such as Fe^{3+} , Fe^{2+} , K^+ , Na^+ , Ba^+ , Cu^{2+} , Pb^{2+} , arginine, cysteine, sucrose, HCl (1M), and NaOH (0.5M) have been obtained from the Merck Co. (Germany). Deionized (DI) water was purified using a Milli-Q system.

The size and surface potential of nanoparticles have been tested by dynamic light scattering (DLS) and zeta potential sizer (Horiba SZ-100). Atomic force microscopy (AFM) has been performed using a DME instrument (Dualscope C-26 with DME-SPM 2.1.1.2 software). The functional groups and chemical structure of CDs have been identified by Fourier transform infrared spectroscopy (FTIR) (ABB Bomen, USA) and X-ray powder diffraction (XRD) (Philips PW1730). The morphology of them has been characterized by a transmission electron microscope (TEM TEC9G20, FEI Co., USA) which was recorded at a voltage of 200 kV. The total concentrations of carbon, nitrogen, hydrogen, oxygen, and sulfur have been recorded by an elemental analysis (LECO TruSpec). Moreover, fluorescence spectra and UV-visible spectra have been analyzed by fluorescence spectrophotometry (PerkinElmer LS45) and an UV-visible spectrophotometer (PerkinElmer Lambda 2), respectively.

2.2. Synthesis of CDs

CDs have been synthesized for first time from *Prunus italica Borkh*. Obtained fruit juice from this green source has been transferred into a Teflon-lined autoclave and heated at 180 °C for 8 h. Afterward, the autoclave has been allowed to cool down. The supplied juice solution has been centrifuged at 8000 rpm for 10 min to remove their impurities [28]. Finally, obtained brown solution has been freeze-dried (Christ Alpha 3-4 LSCbasic, Martin Christ GmbH, Germany) and stored at -80 °C for further investigations.

2.3. Characterization of CDs

DLS and zeta potential sizer ascertain the size and surface charge of CDs, respectively. The morphology of CDs has been displayed by AFM and TEM. The surface functional groups of CDs have been identified by FTIR and the chemical structure of them has been analyzed by XRD, and CHNS/O elemental analysis test.

2.4. Optical features of CDs

The excitation wavelength has a significant impact on the fluorescent emission spectra of multicolor CDs. Therefore, the emission spectra of each separate concentration of CDs (0.003-1 mg/mL) were scanned using a slit width of 20 nm by photoluminescence (PL) spectrophotometer. Furthermore, at maximum excitation, the emission spectra of CDs have been recorded. Suitable concentrations of multicolor CDs for each of the fluorescence color have been chosen according to the maximum fluorescence intensity at their emission wavelengths.

2.5. Quantum-yield (QY) measurements

The ratio of absorbed photons to emitted photons has been recognized as fluorescence QY compared with quinine sulfate as reference ($\phi = 0.54$ in 0.05 H₂SO₄). The QY has been calculated using Equation 1 [32].

$$\phi_X = \phi_S \times A_s/A_x \times F_x/F_s \times (n_x/n_s)^2 \quad (1)$$

Which (X) refers to sample and (S) refers to quinine sulfate, ϕ is the QY, A is the absorbance at the excitation wavelength of 365 nm, F is the integrated emission intensity, and n is the solvent refraction index (1.33 for water) [32].

2.6. pH effect of CDs

To investigate the pH-responsive behavior of CDs, different solutions with different pH values, from 3 to 12, have been prepared by NaOH (0.5 M) and HCl (1M). Then, the PL intensity of them has been measured by the fluorescence spectrophotometer.

2.7. Impact of time and temperature on CDs

To scrutinize the optimum temperature and time of CDs, initially the fluorescence intensity spectra of them have been measured at different temperatures, including -80, -20, 4, 25, 45, and 75 °C by the fluorescence

spectrophotometer. Besides, the PL spectra of CDs at 25 °C during different periods time, such as 0 day, 1, 3, 6, and 9 months have been investigated. It should be mentioned that in this experiment the period time of 0 day is considered as control group.

2.8. Preparation of metal ions solutions

To examine the process of Fe(III) detection by CDs, a wide range of CDs concentrations have been prepared, from 0.06 to 500 μ M and the quenching behavior of them have been assessed in the presence of Fe(III). Additionally, to examine the high selectivity of designed nanosensor in this study, Fe²⁺, Ba⁺, K⁺, Na⁺, Cu²⁺, Pb²⁺, arginine, cysteine, and sucrose have been tested at same concentrations of Fe(III) (0.06-500 μ M). Eventually, the PL spectra of CDs solutions mixed with each of mentioned metal ions have been measured. Each of prepared solution has been also tested under the UV light.

2.9. Preparation of metal ions solutions in real sample

In the present study, tap water and cysteine solution have been considered as real samples so as to validate the specificity of Fe(III) detection. Subsequently, various concentrations of Fe(III) (0.06 - 500 μ M) have been added to the tap water samples mixed with CDs and cysteine solution mixed with CDs, separately. Moreover, the PL intensity of every prepared solution has been investigated by both the UV light and PL spectra spectrophotometer.

2.10. Statistical analysis

In this study, we run analyses of variance (ANOVA) by IBM SPSS 26.0 software in triplicate with a significance value at $P \leq 0.05$.

3. Results and Discussion

3.1. Characterization of CDs

This study is the first to synthesize CDs from this local fruit as a green source by hydrothermal method. The average size of 5 nm has been measured by DLS for this synthesized CD (Figure 1a). This reported size is similar to CDs' size range which is less than 10 nm [33]. The surface charge of CDs was evaluated by zeta potential. Figure 1b exhibits a negative charge recorded -0.2 mv which agrees with former studies [20]. From

morphological aspect, AFM analysis illustrated the size and morphology of CDs measure a diameter of 3.66 nm with the 1-3 layers of graphite for the synthesized CDs (Figure 1c). These dimensions and the number of graphite layers also match previous studies [34]. Another test which validates the morphology and size distribution of synthesized CDs is TEM. As illustrated by Figure 1d, TEM images indicate a size distribution between 2 and 8 nm with the average diameter of 4 nm that this result also confirms the size range of CDs which is less than 10 nm. The XRD pattern of CDs presents an amorphous and broad peak at $2\theta = 21.13^\circ$ with interlayer spacing of

4.2° . This reported d-spacing is more than that of bulk graphite (3.44°) (Figure 1e). This indicates the amorphous nature and irregular structure of synthesized CDs in this study in line with other CDs (35). As shown by Figure 1f, a wide range of functional groups comprising 3413.19 cm^{-1} for N-H/O-H stretch, 2941.84 cm^{-1} for C-H, 1729.88 cm^{-1} for C=O, 1409.07 cm^{-1} for C=C, 1205.04 cm^{-1} for C-O, and 1072.37 cm^{-1} for C-N have been recorded by FTIR spectra. The elemental analysis also indicates the percentage of the main elements of CDs (Table 1).

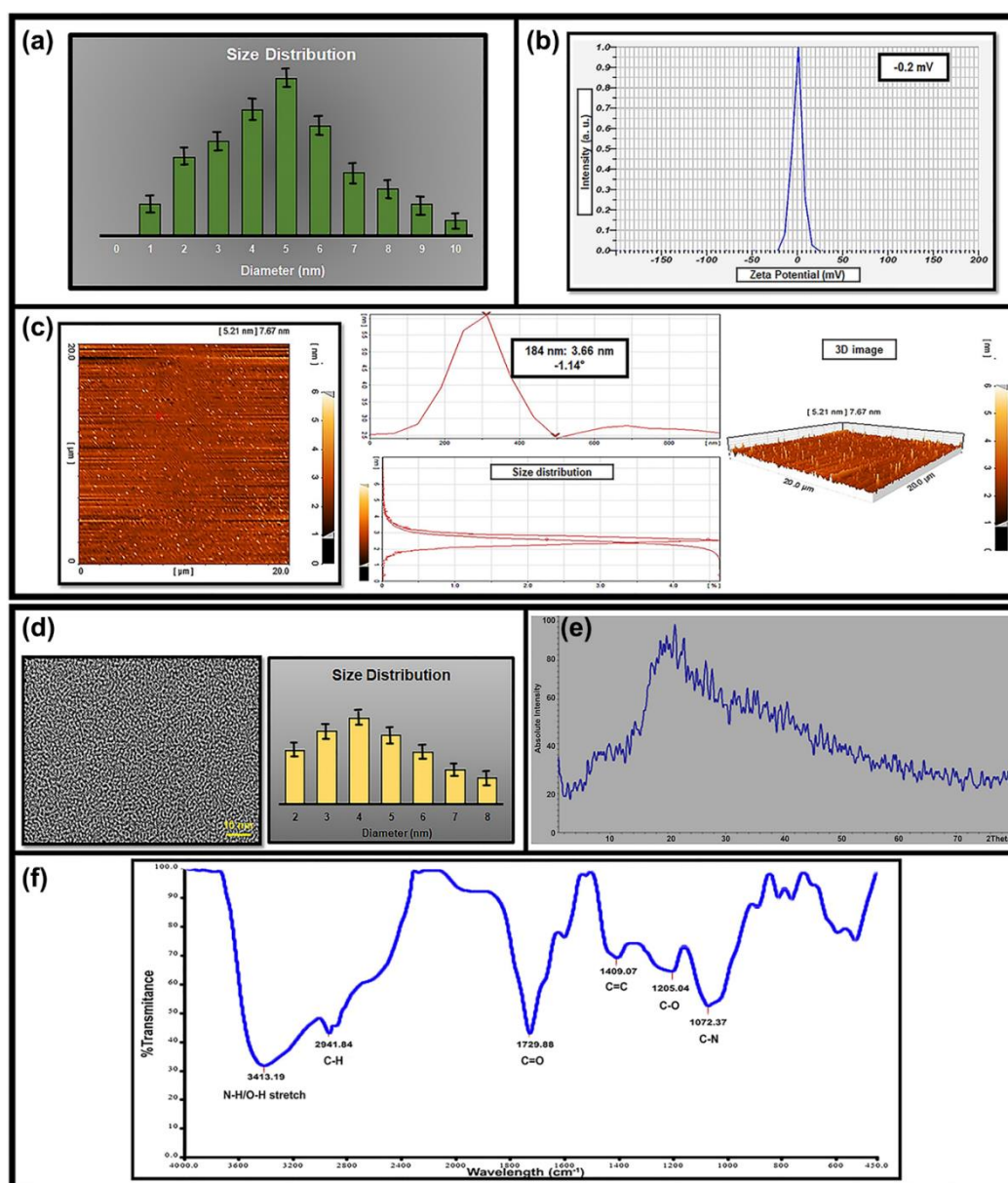


Figure 1: Characterization of CDs. (a) DLS identifying size of CDs; (b) the zeta potential of CDs recording the surface charge of them; the morphology and size distribution of CDs displayed by (c) AFM and (d) TEM; (e) the chemical structure of CDs identified by XRD; (f) different functional groups of CDs determined by FTIR.

Table 1: Elemental analysis of synthesized CDs.

Components	C	N	H	S	O
Elements (%)	40.3	5	6	-	48.7

3.2. Optical features and QY measurement of CDs

Since the change of CDs concentrations brings about a color change in them, the emission spectra of each of CD concentration (0.003-1 mg/mL) have been scanned using a slit width of 20 nm (Figure 2a-l). The emitted PL varied according to CD concentrations, being red (1 mg/mL) (Figure 2a), yellow (0.33, 0.2, and 0.14 mg/mL) (Figure 2b-d), green (0.11, 0.06, and 0.03 mg/mL) (Figure 2e-g), and blue (0.015, 0.012, 0.01, 0.007, and 0.003 mg/mL) (Figure 2h-l). Therefore, the CDs concentrations have been categorized into four classifications (Figure 2m-p). Our results illustrate that the maximum fluorescence intensity of red (1mg/mL) (Figure 2m), yellow (0.14 mg/mL) (Figure 2n), green (0.06 mg/mL) (Figure 2o), and blue CDs (0.012 mg/mL) (Figure 2p) at the excitation wavelength of 500, 460, 420, and 360 nm, respectively, produced maximum emissions at 570, 500, 485, and 460 nm, respectively. These results indicate the concentrations-dependent behavior of synthesized multicolor CDs in this study which is considered as a unique property of them. In present study, since blue CDs (excitation wavelength: 360 nm, emission wavelength: 460 nm) display a higher fluorescence intensity than other colors, it is selected as the suitable CDs for designing nanobiosensor in order to sense Fe (III).

The UV-Visible spectra of CDs represent an extensive absorbance band at 280 nm which reflects $n-\pi^*$ and $\pi-\pi^*$ transition of the C=O bonds and conjugated C=C bonds (Figure 2q). These observations are in line with previous studies [36].

Our data illustrate a 33 % fluorescent QY. Given reported QY, this result can be considered as in a high range of QY measurements of CDs [37].

3.3. pH effect on CDs

As depicted by Figure 3, PL intensity of CDs reaches a peak at pH 5 and then falls to pH 12. These results validate the pH-responsive behavior of synthesized CDs in this study such as some previous studies [38]. Therefore, CDs solution with pH 5 has been chosen for further investigations in this research.

3.4. Impact of time and temperature on CDs

To ascertain the optimum temperature of CDs, the fluorescence intensity spectra of them at -80, -20, 4, 25, 45, and 75 °C have been measured. As displayed by Figure 4a, a significant decrease in the fluorescence intensity of CDs at 45 and 75 °C has been illustrated in comparison with other temperatures. Nonetheless, CDs kept at -80, -20, 4, and 25 °C display higher PL intensity compared with other recorded temperatures. These results indicate that the PL intensity of proposed CDs in this study declines upon raising the temperature from 40 to 70 °C and the optimum temperature of our designed CDs is devoted to colder temperatures, such as most previous studies [39]. This result indicates the significant impact of really low temperatures on the PL intensity of synthesized CDs in this study and confirms the temperature-dependent behavior of proposed CDs. Since CDs at room temperature exhibit the high PL intensity as well as other low temperatures, the variation of time on the PL intensity of CDs has been investigated at 25 °C. As displayed by Figure 4b, there is no significant difference between the PL intensity of CDs after 1, 3, and 6 months in comparison with control group of this study. However, after 9 months, a slight decline in the fluorescence intensity of CDs has been illustrated (Figure 4b). In spite of temperature-sensitive behavior of CDs, these results indicate that they can display the high photostability. There are less CDs that can indicate both two features together [40, 41]. This kind of CDs synthesized in this study can be considered as an efficient nanoparticle due to displaying of both mentioned properties together.

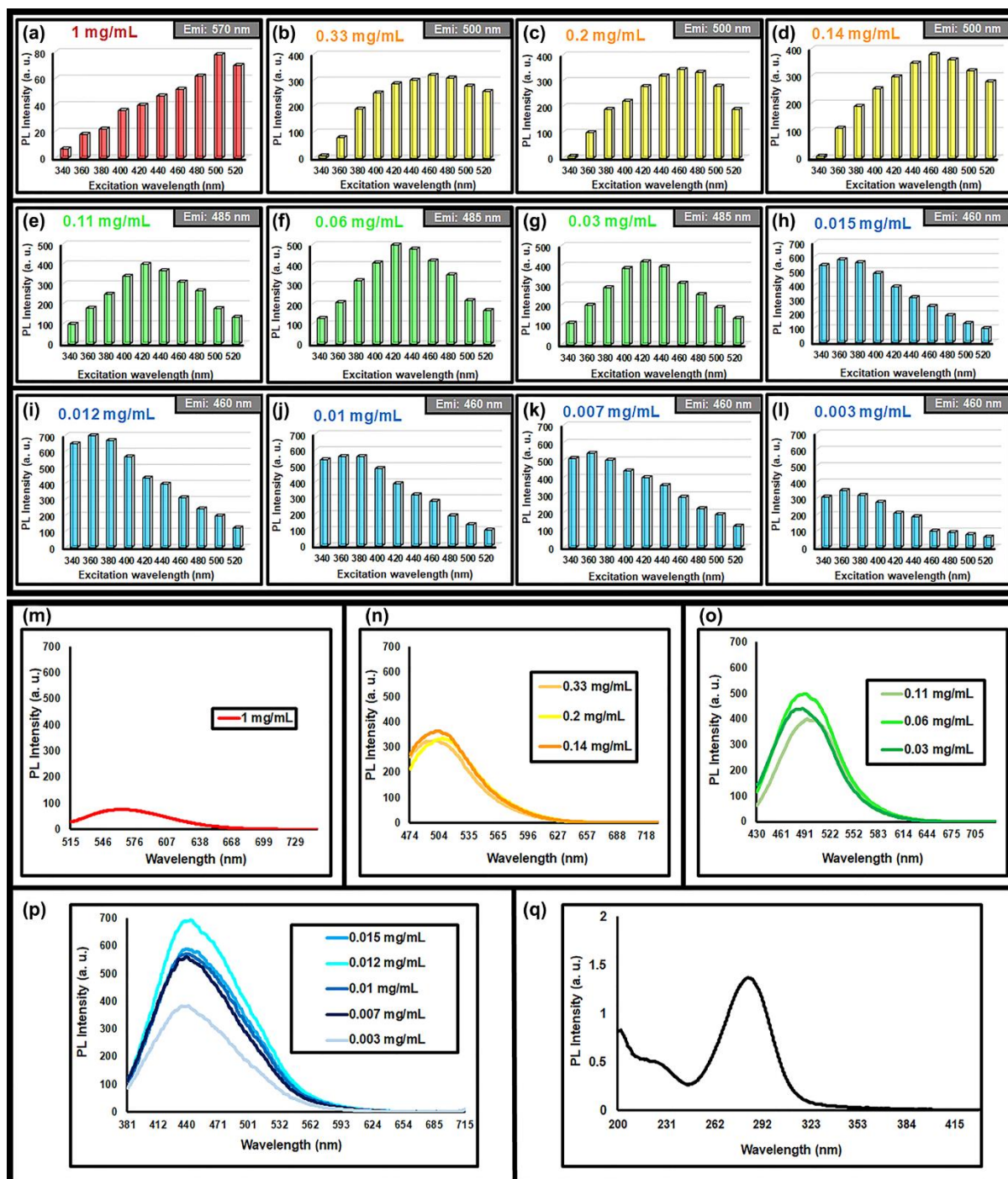


Figure 2: The emission spectra scan of CDs at different concentrations which exhibit (a) red, (b), (c), (d) yellow, (e), (f), (g) green, and (h), (i), (j), (k), (l) blue colors. (m) PL intensity of CDs at concentration of 1 mg/mL at excitation wavelength of 500 nm; (n) the PL intensity of three concentrations (0.33, 0.2, and 0.14 mg/mL) of CDs at excitation wavelength of 460 nm. (o) the PL intensity of three concentrations (0.11, 0.06, and 0.03 mg/mL) of CDs at excitation wavelength of 420 nm; (p) the PL intensity of five concentrations (0.015, 0.012, 0.01, 0.007, 0.003 mg/mL) of CDs at excitation wavelength of 360 nm and (q) UV-Visible absorbance band of CDs.

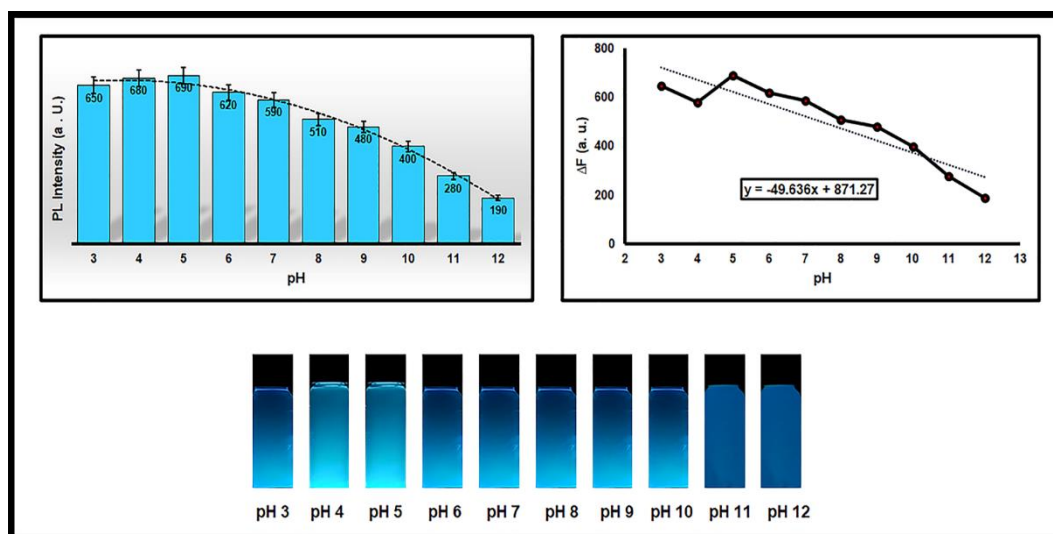


Figure 3: PL intensity of CDs at different pH values.

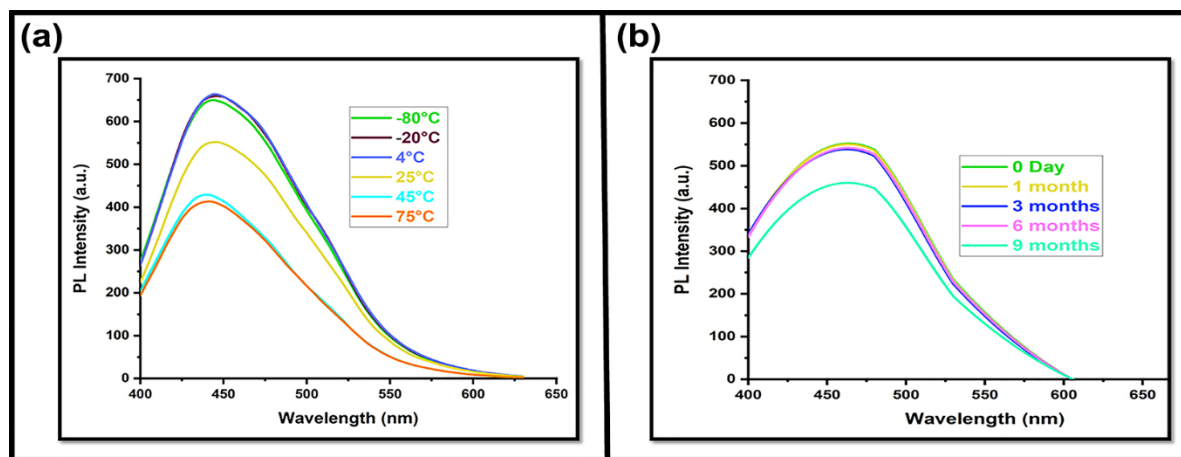


Figure 4: (a) PL intensity of CDs at different temperatures; (b) PL intensity of CDs during different time.

3.5. Detection of Fe (III)

We designed a novel nanobiosensor with interesting optical features for Fe(III) detection through ON-OFF fluorescent system. In the presence of Fe(III), the observed fluorescence quenching in comparison with the fluorescence intensity of CDs can clearly explain the Fe(III) detection (Figure 5a). This finding has been found out by the fluorescence spectroscopy graphs and images taken under the UV light (Figure 5a). As exhibited by Figure 5a, a strong fluorescence emission peak has been recorded at the excitation wavelength of 360 nm devoted to the fluorescence emission of CDs. This can be considered as a positive control in this study. By adding different concentrations of Fe(III) from 0.06 to 500 μM ,

fluorescence quenching can be illustrated. The enhanced fluorescence intensity of the probe system (ΔF) versus Fe(III) concentrations (C) has been plotted with calibration function of $\Delta F = 53.739 \ln(C) + 490.24$ and correlation coefficient (R^2) of 0.954. The detection limit has been measured at 0.06 μM . These findings confirm the functionality of our designed nanobiosensor in this study with the lowest detection limit of any set up biosensors for metal ions detection (Table 2) [42, 43]. It can be concluded that proposed nanobiosensor in this study based on ON-OFF fluorescent probe system can sense Fe(III) more accurately than other nanobiosensors which detect metal ions.

Table 2: Comparison of different fluorescent CDs used for Fe (III) detection.

Analyte	Transducing Method	CDs' Source	CDs' Color	Linear Range	Detection Limit	Real Sample	Ref.
Fe(III)	Fluorescence	Citric acid + Benzoylurea	Blue	5-500 μM	1.1 μM	-	[44]
Fe(III)	Fluorescence	aluminum (III)-2,2'- dihydroxyazobenzene (DHAB) + Acetate buffer solution	Blue	3.5×10^{-6} - 6.7×10^{-4} M	1.6×10^{-6} M	Tap water	[45]
Fe(III)	Fluorescence	Diaminobenzenesulfo nic acid	Red	0-30 μM	0.27 μM	Human serum samples	[31]
Fe(III)	Fluorescence	Alginic acid + Ethanediamine (EDA)	Blue	0-0.05 mM	10.98 μM	River water	[8]
Fe(III)	Fluorescence	B-Cyclodextrin	Blue	1×10^{-6} - $5 \times$ 10^{-4} M	1M	-	[40]
Fe(III)	Fluorescence	α -CDs (purchased from sigma Co.) + Sodium hydroxide	Blue	1.6×10^{-5} - 16.6×10^{-5} M	6 μM	Blood serum	[47]
Fe(III)	Fluorescence	L-Aspartic acid + 2,5- diaminobenzenesulfon ic acid	Green	0-1000 μM	1.51 μM	Diluted tap water + Fetal bovine serum	[48]
Fe(III)	Fluorescence	Kentucky Bluegrass	Blue	5-25 μM	1.4 μM	-	[49]
Fe(III)	Fluorescence	Magnolia liliiflora flower	Blue + Green + Red	1-1000 μM	1.2 μM	Cells	[50]
Fe(III)	Fluorescence	Cranberry beans	Blue	30-600 μM	9.55 μM	Real water samples	[51]
Fe(III)	Fluorescence	Water melon Juice	Blue	-	0.16 μM	Cells	[52]
Fe(III)	Fluorescence	Citric acid + 2,2-DPA	Blue	1-300 μM	5.4 μM	Real water samples	[53]
Fe(III)	Fluorescence	L-Glu + Silica gel powder	Blue	-	10^{-5} M	-	[54]
Fe(III)	Fluorescence	<i>Prunus italica</i> Borkh	Blue + Green + Yellow + Red	0.06-500 μM	0.06 μM	Tap water	This Work

Furthermore, to optimize the pH of detecting solutions, the repeatability of Fe(III) detection process at different pH values has been investigated. As shown by Figure 5b, the most quenching rate is devoted to the detection of Fe(III) in the acidic range of pH and a down ward trend can be seen from pH 3 to pH 12. This result completely aligns with the previous investigation about the pH effect on CDs in this study. In addition to the highest PL intensity of CDs devoted to acidic pH, the best quenching process can also be occurred in acidic pH range, like most synthesized CDs in recent studies [55]. This result indicates that the pH range of 3-5 can be considered as an appropriate pH range in this study for further investigations.

3.6. Fe (III) detection in real sample

The fluorescent behavior of CDs in the presence of Fe(III) has been examined in tap water and cysteine solution. As exhibited by Figure 6a and Figure 6b, adding different concentrations of Fe(III) (0.06-500 μM) to tap water and cysteine solution results in significant quenching as well as *in vitro* study with same detection limit. These data justify the repeatability and sensitivity

of our system in both environmental and biological samples. Moreover, the non-linear relationship between fluorescence intensity and Fe(III) concentrations has been plotted and $y = 25.689 \ln(x)+544.67$ and $y = 25.426 \ln(X)+538.33$ equations have been illustrated for tap water and cysteine solution, respectively ($R^2 = 0.9829$, $R^2 = 0.9786$) (Figure 6a and 6b). The addition of CDs to tap water (T-CDs) has been considered as positive control which depict a strong fluorescence peak at excitation wavelength of 360 nm.

Spiking levels of Fe (III) (0.24, 1, 100 μM) in Fe(III)-free tap water and cysteine solution samples have performed. Suitable recoveries range of Fe (III) from 95.8 % to 99.95 % and from 93.75 % to 99.96 % along with relative standard deviation (RSD) values ranging from 1.95 % to 2.9 % and from 1.96 % to 2.83 % have been evaluated in tap water and cysteine solution as real samples, respectively (Table 3). Ultimately, the high repeatability and reliability of our novel nanobiosensor in this study have been confirmed by the amazing results of recovery and RSD values of Fe(III) in this study in comparison with previous studies [38, 56].

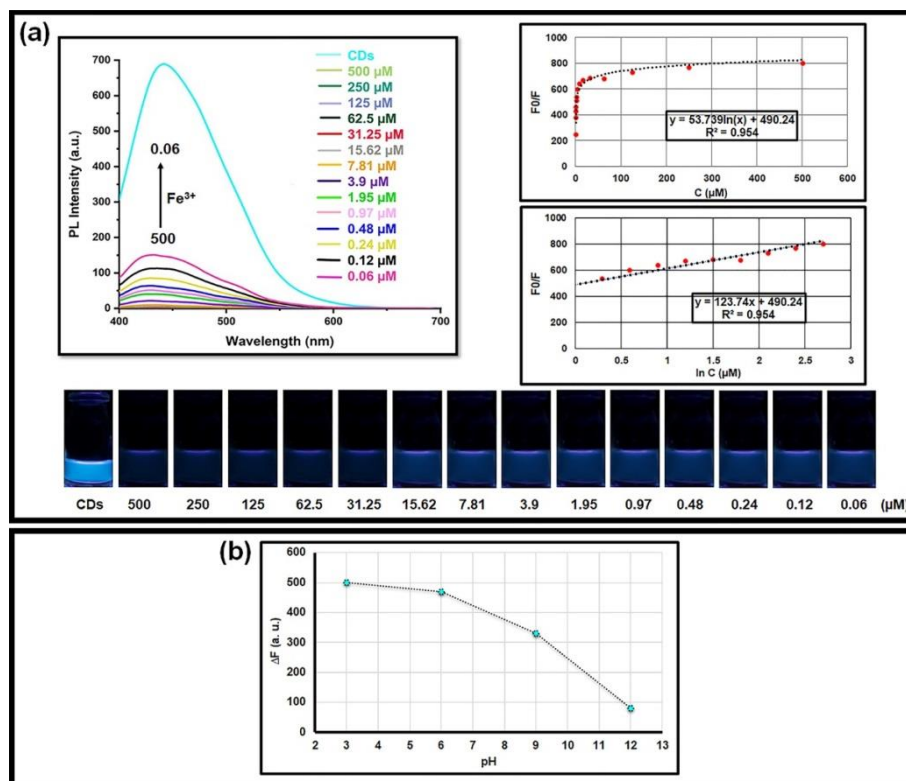


Figure 5: Fe(III) detection by CDs. (a) Different concentration of Fe(III) which are detected by CDs. The images display quenching intensities at innumerable concentrations as observed by under UV light. The non-linear and linear relationship between fluorescence intensity and Fe(III) concentrations is plotted with $y = a \ln(x)+b$ and $y = ax + b$ equations, respectively. (b) Fluorescence intensity of CDs in the presence of Fe(III) at pH of 3, 6, 9, and 12.

Table 3: Results of Fe (III) detection in tap water as a real sample.

Sample	Spiked Concentration (μM)	Found Concentration (μM)	Recovery (%)	RSD (% , n=5)
Tap water 1	0.24	0.23	95.8	2.9
Tap water 2	1	1.01	99	2.1
Tap water 3	100	99.95	99.95	1.95
Cysteine solution 1	0.24	0.225	93.75	2.83
Cysteine solution 2	1	0.98	98	2.2
Cysteine solution 3	100	99.96	99.96	1.96

3.7. Selectivity of Fe (III) detection

The selectivity of designed nanobiosensor has been designed by the examination of the PL intensity change of CDs toward Fe^{2+} , Ba^+ , K^+ , Na^+ , Cu^{2+} , Pb^{2+} , arginine, cysteine, and sucrose. These metal ions illustrate no significant impact on the PL intensity of CDs compared with Fe(III) (Figure 6c). This means these metal ions did not quench emitted fluorescence light of CDs. Calculated quenching rates of CDs in the presence of above-mentioned ions have been measured by Equation 2 [57] and their graphs have been shown by Figure 6c.

$$QR = F_0 - F / F_0 \quad (2)$$

By equation 2, quenching rate, PL intensity of CDs in the absence and presence of different analytes have been reported by QR , F_0 , and F , respectively.

As exhibited by Figure 6c, observed considerable difference between quenching rates of Fe(III) and other ions can validate the specific recognition of our CDs to determine Fe (III).

3.8. Quenching mechanism

The fluorescence quenching mechanism of fluorescent probes can be explained by Stern-Volmer equation (equation 3) [58]:

$$F_0/F = 1 + K_{sv} [Q] \quad (3)$$

where F and F_0 are the fluorescence intensities of CDs in the presence and absence of Fe(III), respectively, and $[Q]$ and K_{sv} are the quencher concentration and the Stern–Volmer quenching

constant, respectively [59]. The linear relationship of F_0/F plot as a function of $[Q]$ validates the Stern–Volmer concept [28]. Plots of PL intensity (F_0/F) versus the concentrations of Fe(III) depicted by Figure 5a and 6a indicate a non-linear relationship and an upward trend. This observed pattern can propose the static quenching mechanism as a probable quenching process for this study.

Furthermore, inner filter effect (IFE) quenching mechanism as another option has been investigated. As displayed by Figure 7a, the UV-visible absorption spectra of Fe(III) as a quencher do not overlap with the emission spectra of CDs at the emission wavelength of 460 nm. Hence, IFE quenching mechanism is rejected. An effective method in order to distinguish static quenching mechanism from dynamic quenching mechanism is the UV-Visible absorption peak of the quencher and CD-quencher system according to previous studies [28]. In this way, when a shift between the UV-visible spectra of quencher and CDs-quencher complex can be illustrated, it can be mentioned that ground-state complex can be performed and static quenching is occurred [61-63]. Figure 7b confirms the formation of ground-state complex in this study. Additionally, as shown by Figure 7b, the graph of CD-Fe^{3+} and CD+Fe^{3+} which is the summed absorption spectra of CD and Fe^{3+} do not coincide with each other that this concept can indicate the formation of ground-state complex between Fe^{3+} and CDs in this study [62, 64, 65]. Eventually, these results justify the static quenching mechanism of Fe^{3+} detection system by CDs proposed in this research and the schematic illustration of this quenching system is exhibited by Figure 7c.

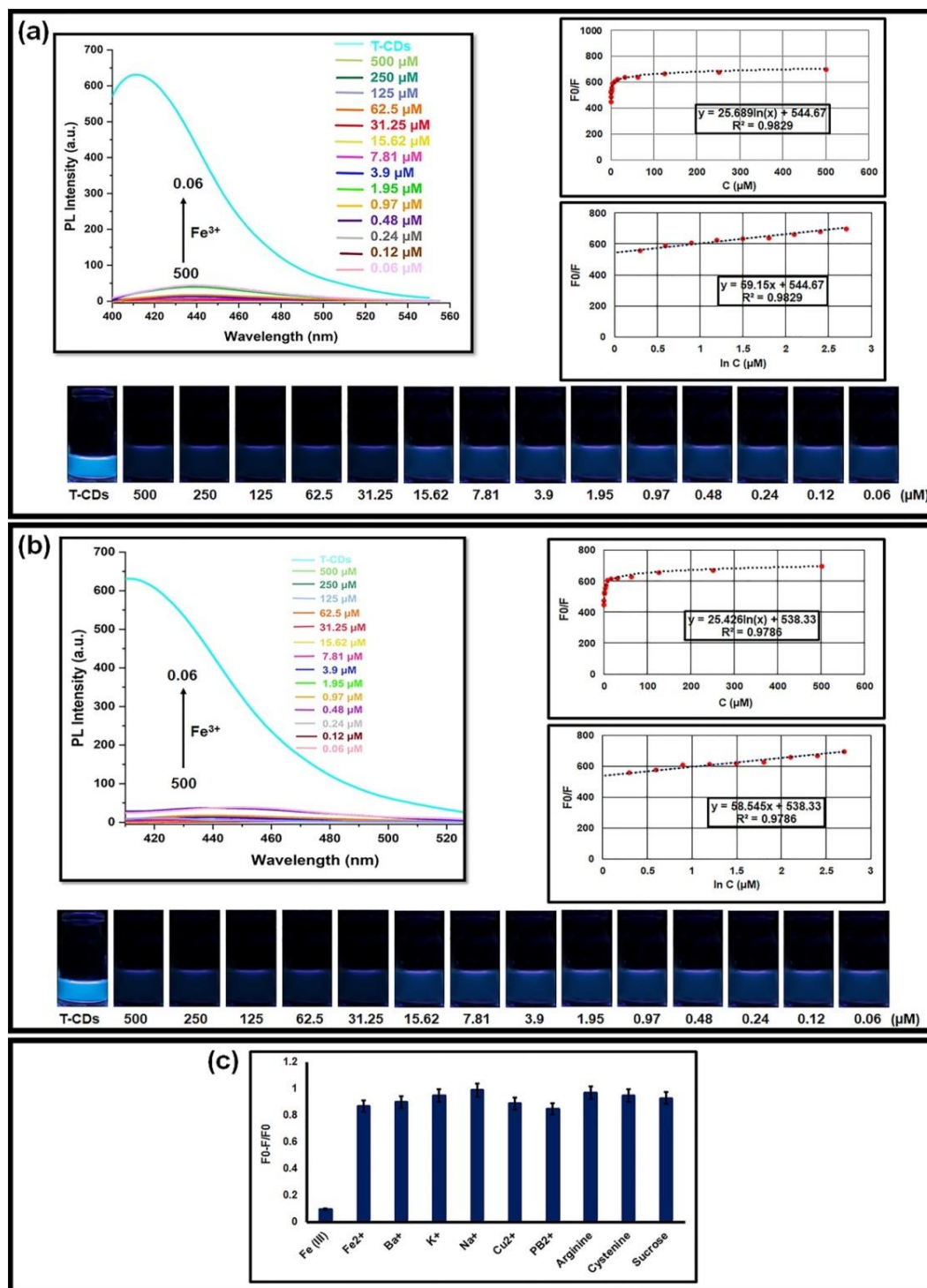


Figure 6: Fe(III) detection by CDs in real sample and selectivity test of CDs. Different concentration of Fe(III) which are determined in (a) tap water and (b) cysteine solution. The images display quenching intensities at innumerable concentrations as observed by under UV light. The non-linear and linear relationship between fluorescence intensity and Fe(III) concentrations is plotted with $y = a \ln(x) + b$ and $y = ax + b$ equations, respectively. (c) Fe^{2+} , Ba^+ , K^+ , Na^+ , Cu^{2+} , Pb^{2+} , arginine, cysteine, and sucrose are considered to examine the fluorescent quenching rate of synthesized CDs.

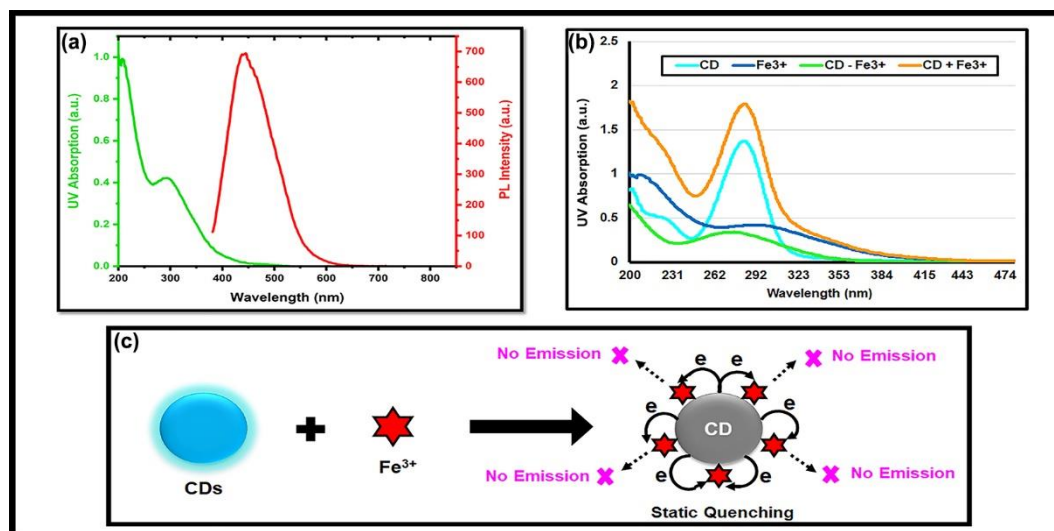


Figure 7: (a) The UV absorption spectra of Fe(III) do not overlap with the PL spectra of CDs at the emission wavelength of 460 nm, indicating the rejection of IFE quenching mechanism; (b) Justifying the static quenching system because the UV graph of CD-Fe(III) and CD + Fe(III) do not coincide with each other; (c) Schematic figure of static quenching mechanism of CDs by Fe(III) ions.

4. Conclusion

In this inquiry, we synthesized a novel nanobiosensor based on concentration-dependent multicolor CDs via hydrothermal method. Fe(III) as a common ion in the nature, organisms' bodies, and industry can be detected by our ON-OFF synthesized nanobiosensor with the detection limit of 0.97 μM by their recognition signal which is fluorescence quenching. Our reported detection limit is significantly lower and more accurate

than any developed nanobiosensors for ions detection. The emitted fluorescence light of CDs remained on in the presence of Fe^{2+} , Ba^+ , K^+ , Na^+ , Cu^{2+} , Pb^{2+} , arginine, cysteine, and sucrose. This addresses the high selectivity and accuracy of our nanobiosensor. This indicates that our reported nanobiosensor in this study can play a key role in the future as commercial kits by its sensitivity because Fe(III) detection gives humanity the potential of manufacturing industrial products.

5. References

- Alvandi N, Rajabnejad M, Taghvaei Z, Esfandiari N. New generation of viral nanoparticles for targeted drug delivery in cancer therapy. *J Drug Target*. 2022; 30(2): 151-165. <https://doi.org/10.1080/1061186X.2021.1949600>.
- Taherian A, Esfandiari N, Rouhani S. Breast cancer drug delivery by novel drug-loaded chitosan-coated magnetic nanoparticles. *Cancer Nanotechnol*. 2021;12(1): 1-20. <https://doi.org/10.1186/s12645-021-00086-8>.
- Wan X, Li S, Zhuang L, Tang J. 1-Tryptophan-capped carbon quantum dots for the sensitive and selective fluorescence detection of mercury ion in aqueous solution. *J Nanoparticle Res*. 2016; 18(1): 1-9. <https://doi.org/10.1007/s11051-016-3441-y>.
- Pajewska-Szmyt M, Buszewski B, Gadzała-Kopciuch R. Sulphur and nitrogen doped carbon dots synthesis by microwave assisted method as quantitative analytical nano-tool for mercury ion sensing. *Mater Chem Phys*. 2020; 242(15): 122484. <https://doi.org/10.1016/j.matchemphys.2019.122484>.
- Zhang S, Jin L, Liu J, Wang Q, Jiao L. A label-free yellow-emissive carbon dot-based nanosensor for sensitive and selective ratiometric detection of chromium (VI) in environmental water samples. *Mater Chem Phys*. 2020; 248(1): 122912. <https://doi.org/10.1016/j.matchemphys.2020.122912>.
- Wang C, Wang Y, Shi H, Yan Y, Liu E, Hu X, Fan J. A strong blue fluorescent nanoprobe for highly sensitive and selective detection of mercury(II) based on sulfur doped carbon quantum dots. *Mater Chem Phys*. 2019; 232(15): 145-151. <https://doi.org/10.1016/j.matchemphys.2019.04.071>.
- Gumpu MB, Sethuraman S, Krishnan UM, Rayappan JBB. A review on detection of heavy metal ions in water - An electrochemical approach. *Sensors Actuators B Chem*. 2015; 213(5): 515-533. <https://doi.org/10.1016/j.snb.2015.02.122>.
- Liu Y, Liu Y, Park SJ, Zhang Y, Kim T, Chae S, Park M, Kim HY. One-step synthesis of robust nitrogen-

- doped carbon dots: Acid-evoked fluorescence enhancement and their application in Fe³⁺ detection. *J Mater Chem A*. 2015; 3(10): 17747-17754. <https://doi.org/10.1039/C5TA05189D>.
9. Fatahi Z, Esfandiari N, Ranjbar Z. A new anti-counterfeiting feature relying on invisible non-toxic fluorescent carbon dots. *J Anal Test*. 2020; 4(1): 307-315. <https://doi.org/10.1007/s41664-020-00149-6>.
 10. Esfandiari N, Arzanani M, Biology MST. A new application of plant virus nanoparticles as drug delivery in breast cancer, *Tumor Biol*. 2016; 37(1): 1229-36. <https://doi.org/10.1007/s13277-015-3867-3>.
 11. Esfandiari N, Taherian A. Nanomedicine, A New Therapeutic Strategy in Breast Cancer treatment, *Arch Breast Cancer*. 2019; 6(2): 69-82. <https://doi.org/10.32768/abc.201962567-78>.
 12. Rommasi F, Esfandiari N. Liposomal nanomedicine: applications for drug delivery in cancer therapy. *Nanoscale Res Lett*. 2021; 16 (1): 95-104. <https://doi.org/10.1186/s11671-021-03553-8>.
 13. Esfandiari N, Arzanani MK, Koochi-Habibi M. The study of toxicity and pathogenicity risk of Potato virus X/herceptin nanoparticles as agents for cancer therapy. *Cancer Nanotechnol*. 2018; 9(1): 1-13. <https://doi.org/10.1186/s12645-018-0036-6>.
 14. Esfandiari N, Sefidbakht Y. An isolate of Potato Virus X capsid protein from *N. benthamiana*: Insights from homology modeling and molecular dynamics simulation. *Int J Biol Macromol*. 2018; 116(3): 939-946. <https://doi.org/10.1016/j.ijbiomac.2018.05.042>.
 15. Esfandiari N, Kohi-Habibi M, Hohn T, Pooggin MM. Complete genome sequence of an Iranian isolate of potato virus X from the legume plant *Pisum sativum*, *Virus Genes*. 2009; 39(1): 141-145. <https://doi.org/10.1007/s11262-009-0371-0>.
 16. Esfandiari N. Targeting breast cancer with bio-inspired virus nanoparticles. *Arch Breast Cancer*. 2018; 5(2): 90-95. <https://doi.org/10.19187/abc.20185290-95>.
 17. Dong W, Hu X, Chen Z, Duan D, Wu Q. An innovative bio-tissue network signal amplifier activated by high-N-doped carbon for uric acid detection. *Mater Chem Phys*. 2020; 254(1): 123295. <https://doi.org/10.1016/j.matchemphys.2020.123295>.
 18. Wu Y, Wu Y, Lv X, Lei W, Ding Y, Chen C, Lv J, Feng S, Chen SM, Hao Q. A sensitive sensing platform for acetaminophen based on palladium and multi-walled carbon nanotube composites and electrochemical detection mechanism. *Mater Chem Phys*. 2020; 239(1): 121977. <https://doi.org/10.1016/j.matchemphys.2019.121977>.
 19. Yin Y, Zhang Y, Gao T, Yao T, Han J, Han Z, Zhang Z, Wu Q, Song B. One-pot evaporation–condensation strategy for green synthesis of carbon nitride quantum dots: An efficient fluorescent probe for ion detection and bioimaging. *Mater Chem Phys*. 2017; 194(1): 293-301. <https://doi.org/10.1016/j.matchemphys.2017.03.054>.
 20. Tafreshi FA, Fatahi Z, Ghasemi SF, Taherian A, Esfandiari N. Ultrasensitive fluorescent detection of pesticides in real sample by using green carbon dots. *PLOS One*. 2020; 15(1): 1-17. <https://doi.org/10.1371/journal.pone.0230646>.
 21. Lv P, Yao Y, Zhou H, Zhang J, Pang Z, Ao K, Cai Y, Wei Q. Synthesis of novel nitrogen-doped carbon dots for highly selective detection of iron ion. *Nanotechnol*. 2017; 28(16): 165502. <https://doi.org/10.1088/1361-6528/aa6320>.
 22. Wang M, Li M, Lu J, Fan B, He Y, Wang F. Advances pesticides using a carbon dot-Au (III) complex. *RCS*. 2018; 4(6): 11551-11556.
 23. Esfandiari N, Bagheri Z, Ehtesabi H, Fatahi Z, Tavana H, Latifi H. Effect of carbonization degree of carbon dots on cytotoxicity and photo-induced toxicity to cells. *Heliyon*. 2019; 5(12): e02940. <https://doi.org/10.1016/j.heliyon.2019.e02940>.
 24. Rahal M, Atassi Y, Ali NN, Alghoraibi I. Novel microwave absorbers based on polypyrrole and carbon quantum dots. *Mater Chem Phys*. 2020; 255(15): 123491. <https://doi.org/10.1016/j.matchemphys.2020.123491>.
 25. Sheng Qian Z, Yue Shan X, Jing Chai L, Rong Chen J, Feng H. Dual-colored graphene quantum dots-labeled nanoprobe/graphene oxide: Functional carbon materials for respective and simultaneous detection of DNA and thrombin, *Nanotechnol*. 2014; 25(41): 415501. <https://doi.org/10.1088/0957-4484/25/41/415501>.
 26. Rashidi E, Esfandiari N, Ranjbar Z, Alvandi N. Designing of a pH-activatable carbon dots as a luminescent nanoprobe for recognizing folate receptor-positive cancer cells. *Nanotechnol*. 2022; 33(7): 44-56. <https://doi.org/10.1088/1361-6528/ac385b>.
 27. Alvandi N, Asgari Z, Bazargannia P, Boushehri YS, Esfandiari N. Treatment and diagnosis roles of nanoparticles against SARS-Cov-2, *J Nanostruct.*, 2022; 12(4): 807-825. <https://doi.org/10.22052/JNS.2022.04.004>.
 28. Alvandi N, Assariha S, Esfandiari N. Off-on sensor based on concentration-dependent multicolor fluorescent carbon dots for detecting pesticides. *Nano Struct Nano Object*. 2021; 26(1): 100706. <https://doi.org/10.1016/j.nanoso.2021.100706>.
 29. Wang G., Pan X, Gu L, Ren W, Cheng W. Fluorescent carbon dot (C-dot) nanoclusters. *Nanotechnol*. 2014; 25(37): 375601. <https://doi.org/10.1088/0957-4484/25/37/375601>.
 30. Qin J, Zhang L, Yang R. Solid pyrolysis synthesis of excitation-independent emission carbon dots and its application to isoniazid detection. *J Nanoparticle Res*. 2019; 21(1): 59-63. <https://doi.org/10.1007/s11051-019-4503-8>.
 31. Yang X, Cui F, Ren R, Sun J, Ji J, Pi F, Zhang Y, Sun X. Red-emissive carbon dots for “switch-on” dual function sensing platform rapid detection of ferric ions and l-cysteine in living cells. *ACS Omega*. 2019; 4(7):

- 12575-12583. <https://doi.org/10.1021/acsomega.9b01019>.
32. Ding H, Wei JS, Zhong N, Gao QY, Xiong HM. Highly efficient red-emitting carbon dots with gram-scale yield for bioimaging. *Langmuir*. 2017; 33(44): 12635-12642. <https://doi.org/10.1021/acs.langmuir.7b02385>.
 33. Li M, Yao W, Liu J, Tian Q, Liu L, Ding J, Xue Q, Lu Q, Wu W. Facile synthesis and screen printing of dual-mode luminescent NaYF₄:Er,Yb (Tm)/carbon dots for anti-counterfeiting applications. *J Mater Chem C*. 2017; 5(1), 6512-6520. <https://doi.org/10.1039/C7TC01585B>.
 34. Pan D, Zhang J, Li Z, Wu M. Hydrothermal route for cutting graphene sheets into blue-luminescent graphene quantum dots. *Adv Mater*. 2010; 22(6): 734-738. <https://doi.org/10.1002/adma.200902825>
 35. Mewada A, Pandey S, Shinde S, Mishra N, Oza G, Thakur M, Sharon M, Sharon M. Green synthesis of biocompatible carbon dots using aqueous extract of *Trapa bispinosa* peel. *Mater Sci Eng C*. 2013; 33(5): 2914-2917. <https://doi.org/10.1016/j.msec.2013.03.018>.
 36. Fatahi Z, Esfandiari N, Ehtesabi H, Bagheri Z, Ranjbar Z, Latifi H. Physicochemical and cytotoxicity analysis of green synthesis carbon dots for cell imaging. *EXCLI J*. 2019; 13: 454-466. <https://doi.org/10.17179/excli2019-1465>.
 37. Sharma V, Tiwari P, Mobin SM. Sustainable carbon-dots: Recent advances in green carbon dots for sensing and bioimaging. *J Mater Chem B*. 2017; 5: 8904-8924. <https://doi.org/10.1039/C7TB02484C>.
 38. Zheng X, Ren S, Wang L, Gai Q, Dong Q, Liu W. Controllable functionalization of carbon dots as fluorescent sensors for independent Cr(VI), Fe(III) and Cu(II) ions detection. *J Photochem Photobiol A Chem*. 2021; 417(1): 113359. <https://doi.org/10.1016/j.jphotochem.2021.113359>.
 39. Khan WU, Wang D, Wang Y. Highly green emissive nitrogen-doped carbon dots with excellent thermal stability for bioimaging and solid-state LED. *Inorg Chem*. 2018; 57(24): 15229-15239. <https://doi.org/10.1021/acs.inorgchem.8b02524>.
 40. Kumar N, Bogireddy R, Lara J, Rodriguez L, Agarwal V. One-step hydrothermal preparation of highly stable N doped oxidized carbon dots for toxic organic pollutants sensing and bioimaging. *Chem Eng J*. 2020; 401(1),126097. <https://doi.org/10.1016/j.cej.2020.126097>.
 41. Sun Y, Zheng S, Liu L, Kong Y, Zhang A, Xu K, Han C. The cost-effective preparation of green fluorescent carbon dots for bioimaging and enhanced intracellular drug delivery. *Nanoscale Res Lett*. 2020; 15: 55. <https://doi.org/10.1186/s11671-020-3288-0>.
 42. Liang C, Hu X, Wang Y, Zhang Y, Fu G, Li C. Study on luminescence mechanism of nitrogen-doped carbon quantum dots with different fluorescence properties and application in Fe³⁺ detection, *J Nanoparticle Res*. 2021; 23: 101-119. <https://doi.org/10.1007/s11051-021-05208-2>.
 43. Zhang J, Wang J, Fu J, Fu X, Gan W, Hao H. Rapid synthesis of N, S co-doped carbon dots and their application for Fe³⁺ ion detection. *J Nanoparticle Res*. 2018; 20: 41-48. <https://doi.org/10.1007/s11051-018-4141-6>.
 44. Shan F, Xia H, Xie X, Fu L, Yang H, Zhou Q, Zhang Y, Wang Z, Yu X. Novel N-doped carbon dots prepared via citric acid and benzoylurea by green synthesis for high selectivity Fe(III) sensing and imaging in living cells. *Microchem J*. 2021; 167: 106273. <https://doi.org/10.1016/j.microc.2021.106273>.
 45. Kaneko E, Tanno H, Yotsuyanagi T. Ion-pair adsorption film colorimetry of iron (III) in water samples and human serum. *Mikrochim Acta*. 1991; 103: 37-44. <https://doi.org/10.1007/BF01245050>.
 46. Zhu W, Zhang J, Jiang Z, Wang W, Liu X. High-quality carbon dots: Synthesis, peroxidase-like activity and their application in the detection of H₂O₂, Ag⁺ and Fe³⁺. *RSC Adv*. 2014; 4: 17387-17392. <https://doi.org/10.1039/C3RA47593J>
 47. Hamishehkar H, Ghasemzadeh B, Naseri A, Salehi R, Rasoulzadeh F. Carbon dots preparation as a fluorescent sensing platform for highly efficient detection of Fe(III) ions in biological systems. *Spectrochim Acta Part A Mol Biomol Spectrosc*. 2015; 150: 934-939. <https://doi.org/10.1016/j.saa.2015.06.061>.
 48. Cai H, Xu H, Chu H, Li J, Zhang D. Fabrication of multi-functional carbon dots based on “one stone, three birds” strategy and their applications for the dual-mode Fe³⁺+detection, effective promotion on cell proliferation and treatment on ferric toxicosis: In vitro. *J Mater Chem B*, 2021; 9: 767-782. <https://doi.org/10.1039/D0TB02325F>.
 49. Krishnaiah P, Atchudan R, Perumal S, Salama ES, Lee YR, Jeon BH. Utilization of waste biomass of *Poa pratensis* for green synthesis of n-doped carbon dots and its application in detection of Mn²⁺ and Fe³⁺. *Chemosphere*. 2022; 286(2), 131764. <https://doi.org/10.1016/j.chemosphere.2021.131764>.
 50. Atchudan R, Edison TNJI, Aseer KR, Perumal S, Lee YR. Hydrothermal conversion of *Magnolia liliiflora* into nitrogen-doped carbon dots as an effective turn-off fluorescence sensing, multi-colour cell imaging and fluorescent ink. *Colloids Surf B Biointerfaces*. 2018; 169(1): 321-328. <https://doi.org/10.1016/j.colsurfb.2018.05.032>.
 51. Zulfajri M, Gedda G, Chang CJ, Chang YP, Huang GG. Cranberry beans derived carbon dots as a potential fluorescence sensor for selective detection of Fe³⁺ ions in aqueous solution. *ACS Omega*. 2019; 4(13): 15382-15392. <https://doi.org/10.1021/acsomega.9b01333>.
 52. Lu M, Duan Y, Song Y, Tan J, Zhou L. Green preparation of versatile nitrogen-doped carbon quantum dots from watermelon juice for cell imaging, detection of Fe³⁺ ions and cysteine, and optical thermometry. *J Mol Liq*. 2018; 269(1): 766-774.

- <https://doi.org/10.1016/j.molliq.2018.08.101>.
53. Salimian Rizi V. Ce Pte Us Pt, *Mater. Res. Express.* (2019), 0-12.
54. He G, Xu M, Shu M, Li X, Yang Z, Zhang L, Su Y, Hu N, Zhang Y. Rapid solid-phase microwave synthesis of highly photoluminescent nitrogen-doped carbon dots for Fe³⁺ detection and cellular bioimaging. *Nanotechnol.* 2016; 27(39): 1-10. <https://doi.org/10.1088/0957-4484/27/39/395706>.
55. Shi J, Ni G, Tu J, Jin X, Peng J. Green synthesis of fluorescent carbon dots for sensitive detection of Fe²⁺ and hydrogen peroxide. *J Nanoparticle Res.* 2017; 19(1): 209-218. <https://doi.org/10.1007/s11051-017-3888-5>.
56. Yang M, Liu M, Wu Z, He Y. Carbon dots co-doped with nitrogen and chlorine for “ off-on ” fluorometric determination of the activity of acetylcholinesterase and for quantification of organophosphate pesticides. *Microchim Acta.* 2019; 186: 585-593. <https://doi.org/10.1007/s00604-019-3715-z>
57. Yang L, Zhang X, Wang J, Sun H, Jiang L. Double-decrease of the fluorescence of CdSe/ZnS quantum dots for the detection of zinc (II) dimethyldithiocarbamate (ziram) based on its interaction with gold nanoparticles. *Microchimica Acta.* 2018; 185(10): 472-486. <https://doi.org/10.1007/s00604-018-2995-z>.
58. Zu F, Yan F, Bai Z, Xu J, Wang Y, Huang Y, Zhou X. The quenching of the fluorescence of carbon dots: A review on mechanisms and applications. *Microchim Acta.* 2017; 184(11): 1899-1914. <https://doi.org/10.1007/s00604-017-2318-9>.
59. Ahmed GHG, Laíño RB, Calzón JAG, García MED. Highly fluorescent carbon dots as nanoprobe for sensitive and selective determination of 4-nitrophenol in surface waters. *Microchim Acta.* 2015; 182(8): 51-59. <https://doi.org/10.1007/s00604-014-1302-x>.
60. Zhang HD, Chen AY, Gan B, Jiang H, Gu LJ. Corrosion protection investigations of carbon dots and polydopamine composite coating on magnesium alloy. *J Magnes Alloy.* 2022; 10(5): 1358-1367. <https://doi.org/10.1016/j.jma.2020.11.021>.
61. Zahraee SS, Alvandi N, Ghamari M, Esfandiari N. An ultra-sensitive nano biosensor for 17 β -estradiol detecting using carbon dots. *Nano Struct Nano Object.* 2023; 34: 100951. <https://doi.org/10.1016/j.nanos.2023.100951>.
62. Assariha S, Alvandi N, Rouhani S, Esfandiari N. Bioinspired multicolor carbon dots: comprehensive cytotoxicity, phytotoxicity, and bioimaging in animal cells and plants. *Luminescence,* 2023; 38(5): 554-567. <https://doi.org/10.1002/bio.4482>
63. Bagheri H, Saber-Tehrani M, Shishehbore MR, Shahvazian M. Janus green dye as a new reagent for catalytic kinetic determination of zirconium in ceramic materials. *Prog Color Colorants Coat.* 2010; 3(2): 58-65. <https://doi.org/10.30509/pccc.2010.75773>.
64. Gharagozlou M, Rouhani S. A new reusable mercury-sensitive turn-on nano-chemosensor based on functionalized CoFe₂O₄@SiO₂ magnetic nanocomposite. *Prog Color Colorants Coat.* 2022; 15(2): 75-85. <https://doi.org/10.30509/pccc.2021.166735.1091>.

How to cite this article:

Alvandi N, Ranjbar Z, Esfandiari N. Fe(III) Detection by Multicolor Carbon Dots as Fluorometric Probes. *Prog Color Colorants Coat.* 2024;17(1):11-25. Doi:10.30509/pccc.2023.167138.1218

